Environ. Sci. Technol. **2009,** *43,* 6724–6729

Selective Detection of Hypertoxic Organophosphates Pesticides via PDMS Composite based Acetylcholinesterase-Inhibition Biosensor

WEI ZHAO, PEI-YU GE, JING-JUAN XU,* AND HONG-YUAN CHEN

Key Laboratory of Analytical Chemistry for Life Science, School of Chemistry and Chemical Engineering, Nanjing University, Nanjing 210093, China

Received March 22, 2009. Revised manuscript received June 16, 2009. Accepted July 22, 2009.

We report on a pair of highly sensitive amperometric biosensors for organophosphate pesticides (OPs) based on assembling acetylcholinesterase (AChE) on poly(dimethylsiloxane) (PDMS)−poly(diallydimethylammonium) (PDDA)/gold nanoparticles (AuNPs) composite film. Two AChE immobilization strategies are proposed based on the composite film with hydrophobic and hydrophilic surface tailored by oxygen plasma. The twin biosensors show interesting different electrochemical performances. The hydrophobic surface based PDMS-PDDA/AuNPs/choline oxidase (ChO)/AChE biosensor (biosensor-1) shows excellent stability and unique selectivity to hypertoxic organophosphate. At optimal conditions, this biosensor-1 could measure 5.0×10^{-10} g/L paraoxon and 1.0×10^{-9} g/L parathion. As for the hydrophilic surface based biosensor (biosensor-2), it shows no selectivity but can be commonly used for the detection of most OPs. Based on the structure of AChE, it is assumed that via the hydrophobic interaction between enzyme molecules and hydrophobic surface, the enzyme active sites surrounded by hydrophobic amino acids face toward the surface and get better protection from OPs. This assumption may explain the different performances of the twin biosensors and especially the unique selectivity of biosensor-1 to hypertoxic OPs. Real sample detection was performed and the omethoate residue on Cottomrose Hibiscus leaves was detected with biosensor-1.

Introduction

Organophosphates pesticides (OPs), one group of the most commonly used pesticides in agriculture, can disrupt the cholinesterase enzyme and lead to cholinergic dysfunction and death, which endanger the health of both humans and animals (*1*−*4*). In concern of health and environment, limiting the amount of OPs in agriculture and prohibiting the use of hypertoxic OPs are critical to worldwide countries. Recently, some hypertoxic OPs such as parathion and methyl parathion were banned or severely restricted in agriculture by the United Nations Environment Programme (UNEP) and the Food and Agricultural Organization (FAO) (*5, 6*). In view of major concerns regarding the toxicity of OPs, many techniques have been introduced for monitoring trace levels of these compounds. Gas chromatography (GC) or high-performance liquid chromatography (HPLC) coupled with mass spectrometry (MS) are used as reference methods but present some drawbacks such as complex and time-consuming pretreatments of the samples, requirements of expensive instruments and well-trained operators, and these methods are also restricted to a limited analyte spectrum (*7, 8*). Therefore, searching for sensitive, selective, simple, and rapid methods is urgent.

Biosensor technology emerged in the past decades is well-suited for on-site environmental monitoring of pesticides (*9, 10*). Indirect biosensors based on the modulated biocatalytic activity of acetylcholinesterase (AChE) have been widely developed for monitoring OPs (*11*−*14*). These are referred to as inhibition biosensors since the quantification of OPs is based on the measurement of the decreased enzyme activity after exposure of enzyme to an inhibitor. Various electrochemical and optical biosensors have been developed using this approach (*11*−*13*). Among them, the electrochemical amperometric transducer came to be the principal choice due to its high sensitivity (*15*). The analysis of OPs was achieved principally based on the inhibition of AChE that induced the decrease of oxidation current of the enzymatic reaction products.

Despite many efforts in the development of the AChE-inhibition biosensors, to meet the specific requirements, such as high sensitivity, rapid response, and good stability, further improvement needs to be carried out. Among the consideration of fabrication of the biosensor, immobilization of enzyme onto solid electrode surface is quite crucial since it can greatly influence the performance of biosensor. The most reported immobilization strategies are covalent binding (*16*), physical or chemical adsorption (*17, 18*), and entrapment in different substrate materials (*19, 20*). However, the application of these methods suffers from some drawbacks, such as physical adsorption and entrapment which may cause irregular enzyme assays and also the leakage of enzyme molecules with time, and chemical interaction (covalent binding) which tends to partially change the native structure of AChE and partially denature the activity of enzyme (*10*). Stable immobilization of AChE and protection of the enzyme activity still need persistent efforts. Recently, Abell and coworkers reported an electrostatic adsorption method for oriented immobilization of carbonic anhydrase onto charged surfaces (*21*). With immobilization of carbonic anhydrase on two differently charged surfaces, the access to the active site of the enzyme for inhibitors was distinctly different. It is an effective approach for the control of enzyme activity on solid surface. However, to our knowledge, the oriented adsorption method has not been used for the immobilization of AChE for biosensing application.

As a durable and biocompatible material, the hydrophobic polymer poly(dimethylsiloxane) (PDMS) facilitates the adhesion of cell and proteins (*22, 23*). It is well adapted for the fabrication of microsystems (*24*). Recently, we reported a PDMS−poly(diallydimethylammonium) (PDDA)/gold nanoparticles (AuNPs) composite film, which was an excellent composite for the capture of AChE (*25*). According to the results from electrochemical experiments and morphology characterization, it was concluded that AChE was mainly adsorbed on the composite film via hydrophobic interaction after the adsorption of ChO. Herein, twin PDMS−PDDA/AuNPs/ChO/AChE based bienzyme biosensors were prepared based on both hydrophobic and hydrophilic composite film surfaces for the detection of OPs. We compared the

* Corresponding author fax: 86-25-83597294; e-mail: xujj@nju.edu.cn.

10.1021/es900841n CCC: $40.75
Published on Web 08/05/2009

performance of the two biosensors, and investigated the mechanism of the immobilization based on the results from electrochemical experiments and AChE molecule structure. Finally, the hydrophobic surface based biosensor, which showed better stability and selectivity to hypertoxic OPs, was utilized for the real sample detection for monitoring omethoate residue on leaves of Cottomrose Hibiscus.

Experimental Section

Reagents. AChE (EC 3.1.1.7, from *Electrophorus electricus*, 1052 units/mg), choline oxidase (ChO, EC 1.1.3.17, from alcaligenes species, 31 units/mg) were purchased from Sigma. Sylgard 184 (PDMS) was from Dow Corning (Midland, MI). Gold chloride ($AuCl_3 \cdot HCl \cdot 4H_2O$) was purchased from Shanghai Chemical Regent Co. Ltd. (Shanghai, China). Choline chloride, acetylcholine chloride, and PDDA M_w 100 000−200 000 g mol^{-1} in 20% aqueous solution were purchased from Aldrich. All the OPs were purchased from China Standard Technology Development Corporation. All other reagents were commercially available and of analytical grade. All solutions were prepared with doubly distilled water.

Preparation of PDMS−PDDA/AuNPs/ChO/AChE Modified Electrodes. Bulk gold disk electrodes (200 μm diameter) were abraded with fine SiC paper and polished carefully with 0.3 and 0.05 μm alumina slurry and then sonicated in water and absolute ethanol, respectively. PDMS−PDDA/AuNPs/ChO/AChE modified electrodes were prepared as follows: A mixture of PDDA and PDMS (20% PDDA aqueous solution, PDMS and a curing agent in 7:10:1, by weight ratio) was dripped on the surface of electrodes by spin coating at 2000 rpm/min for 15 min. The structure was cured at 80 °C for 1 h. A nanofilm with approximate 90 nm thickness was formed on the electrode surface, characterized by scanning electron microscopy (SEM). Then, the electrodes were immersed in 0.5% $HAuCl_4$ solution for 8 h, followed by rinsing thoroughly with doubly distilled water. AuNPs with an average diameter of 13 nm were formed in the PDMS−PDDA film reduced by the residual Si−H group on PDMS surface (*26*).

After the formation of PDMS−PDDA/AuNPs film, the electrodes were dipped into a ChO solution (2 unit/mL, dissolved in 0.1 M phosphate buffer solution (PBS) of pH 7.4) for 10 min. Then, PDMS−PDDA/AuNPs/ChO electrodes were immersed in an AChE solution (2 unit/mL, dissolved in 0.1 M PBS of pH 7.4) for 10 min. All the parameters were optimized.

Another biosensor based on hydrophilic surface was also prepared. The procedure of preparing the electrode and constructing PDMS−PDDA/AuNPs was the same as described above. Before the assembly of proteins, PDMS−PDDA/AuNPs modified electrodes were treated with air plasma (Harrick PDC-32G, pressure: 0.5 mbar). Then, the electrodes were immersed in ChO and AChE solutions for 10 min, respectively.

Electrochemical Measurements. Electrochemical experiments were performed on a CHI 660B electrochemical workstation (Shanghai Chenhua Apparatus Corporation, China). All experiments were carried out using a conventional three-electrode system with a gold disk electrode as a working electrode, a platinum foil as an auxiliary electrode, and a saturated calomel electrode as a reference electrode.

UV−visible Absorption Spectroscopic Measurements. Ultraviolet and visible (UV−vis) absorption spectra were recorded with a Lambda 35 UV/vis spectrometer (Perkin-Elmer instruments, USA).

High-Performance Liquid Chromatography (HPLC) Measurements. HPLC detections at 273 nm were carried out on systems consisting of an Shim-pack VP-ODS column (250 mm × 4.6 mm) equipped with Shimadzu SPD-10A UV−vis detector and Shimadzu LC-10AD pump using a mobile phase containing acetonitrile and H_2O (85:15, V/V) with a flow rate of 1 mL/min.

Contact Angle Characterization. The static water contact angles were measured with a commercial instrument (CAM 200, KSV Instruments Ltd., Helsinki, Finland). A distilled water droplet (drop volume 5 μL) was used as the indicator in the experiment to characterize the wetting property of the as-prepared surface of samples.

Results and Discussion

Immobilization of Proteins on the PDMS−PDDA/AuNPs Modified Electrodes. For the enzyme biosensor, the immobilization of enzyme is a crucial procedure since it would greatly influence the performance of biosensor. In 1990, Bourdillon et al. reported the immobilization of glucose oxidase on hydrophobic aluminum oxide via both electrostatic and hydrophobic interactions (*27*), which were proved to be successful techniques for stabilization of the enzyme in the following studies (*28, 29*). Herein, based on the PDMS−PDDA/AuNPs composite film, we took two protocols for the immobilization of AChE, and thus constructed twin biosensors.

One biosensor (biosensor-1) was prepared with immobilization of AChE and ChO on PDMS−PDDA/AuNPs film without any pretreatment, which showed the water contact angle of 112.66°. As reported, AChE was mainly adsorbed on the film via hydrophobic interaction between the enzyme molecule and PDMS (*25*). The other biosensor (biosensor-2) was based on the composite film treated with oxygen plasma. A plasma cleaner (Harrick PDC-32 G, pressure: 0.5 mbar) was used to treat the composite film for 60 s to tailor the property of surface, since the oxygen plasma treatment could introduce polar groups (−OH) on the surface of PDMS and make the surface hydrophilic (*30*). After the treatment, the water contact angle of PDMS−PDDA/AuNPs film changed to 40.03°. The enzyme immobilization procedure was the same as that of biosensor-1, and the driving forces for the adsorption of AChE on hydrophilic PDMS composite film were supposed to be electrostatic attraction and hydrogen bond.

UV−vis absorption spectra were employed for characterization of enzyme immobilization. Based on the absorption band with 277 nm of AChE (Figure 1A), the loading of AChE on the hydrophilic surfaces is calculated as 0.12 unit/mm^2 (calculated from the difference of peak absorbances from Figure 1C), which is about a half of that adsorbed on the hydrophobic surface, 0.25 unit/mm^2 (calculated from the difference of peak absorbances from Figure 1B). The obvious difference of AChE loading might be attributed to the different driving forces between AChE and PDMS−PDDA/AuNPs film surfaces. For comparison, the UV−vis absorption spectra of ChO were also recorded before and after the incubation of hydrophobic and hydrophilic PDMS−HPDDA/AuNPs films modified electrodes in the sample solutions. Based on the distinct absorption bands of ChO with the maximum absorbance at 276 nm (*25*), and the difference of peak absorbencies, the loading of ChO on hydrophobic and hydrophilic composite films were calculated closely as 0.10 unit/mm^2 and 0.11 unit/mn^2, respectively. This means the main driving force for ChO to adsorb on the untreated PDMS−PDDA/AuNPs film is not the same as that of AChE.

Responses of the Twin Biosensors to Acetylcholine. The electrochemical detection performances of the twin biosensors were examined and compared. In the bienzyme system, acetylcholine is catalyzed by AChE and produces acetate and choline, which are then converted by ChO in the presence of oxygen, producing hydrogen peroxide that can be detected by the amperometric transducer. The typical steady-state amperometric response of biosensor-1 is shown in Figure S1, Supporting Information. The linear calibration

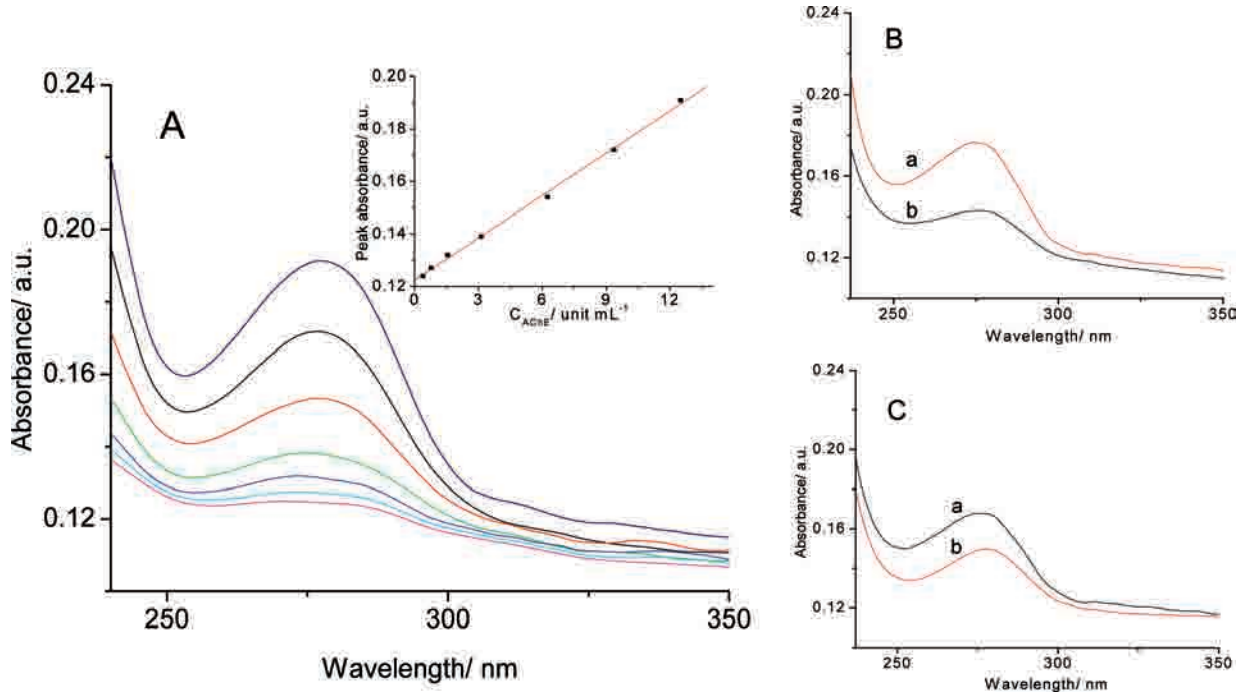

FIGURE 1. UV−visible adsorption spectra of AChE (A) dissolved in 0.1 M pH 7.4 PBS with concentrations increasing from 0.39 to 12.5 unit/mL (from lower to upper), and AChE dissolved in 0.1 M pH 7.4 PBS before (a) and after (b) 10 min incubation of the hydrophobic (B) and hydrophilic (C) PDMS−PDDA/AuNPs film modified electrodes in them, respectively. Inset A: Plot of AChE concentrations vs peak absorbance at 277 nm.

range is 1.0−190 μM ($r = 0.999$, $n = 20$) with a detection limit of 0.3 μM ($S/N = 3$). The time required to reach the 95% steady state response is as fast as within 5 ± 1 s. At the same conditions, the sensitivity to acetylcholine of biosensor-2 is 45.9% compared with biosensor-1, which is close to the conclusions from UV−vis absorption spectra that the loading of AChE on the hydrophilic surface is half of that on the hydrophobic surface.

For the electrochemical biosensors, there are two important environmental factors, pH and temperature, which could greatly influence the sensitivity and stability of the biosensor. Here, we further investigate these factors. It is well-known that both the activity of the immobilized enzymes and the enzymatic reaction are pH-dependent. In pH experiment, the maximum response current of the biosensor-1 to 0.20 mM acetylcholine could be observed between pH 9.0−10.0 (Figure S2A), while biosensor-2 exhibits the maximum response between pH 8.0 and 9.0 (Figure S2B). The effect of pH on the AChE based biosensor resulted from two causes. On one hand, basic condition facilitates oxidation of hydrogen peroxide, and the response of the proposed biosensor will increase with the increase of pH. On the other hand, extreme pH conditions result in the denaturization of enzyme. Here, the immobilized AChE on hydrophobic surface remains active at basic conditions (up to pH 9.0−10.0), indicating that the immobilization protocol in biosensor-1 could well protect the activity of AChE to withstand outside conditions. The environmental temperature could also influence the activity of enzyme and thus affect the performance of the biosensor. For most enzyme biosensors, room temperature was chosen as the operation temperature because at higher temperature, the biostructure of enzyme might be destroyed, which makes it lose the activity permanently. Here, in the temperature influence studies, the responses of biosensor-1 and biosensor-2 to 0.2 mM acetylcholine in 0.1 M pH 9.0 borate buffer solutions at different temperatures were examined. For biosensor-1, a maximum response current was observed at about 40 °C (Figure S2C). And for biosensor-2, the maximum response occurred at about 30 °C (Figure S2D). Therefore, it is noted that the enzyme immobilized on biosensor-1 showed more stability and activity under temperature higher than 25 °C.

In operational stability studies, biosensor-1 shows excellent stability with no decrease in the activity of enzymes for 50 repeated measurements (RSD = 4.9%) in two days. As for biosensor-2, the response to 0.20 mM acetylcholine decreased to 83% of original response current after 50 repeated measurements.

Here it can be concluded that the adsorption of AChE on hydrophobic surface of PDMS composite film provides a more stable immobilization and better protection of enzyme activity.

Application of AChE-Inhibition Biosensors: Detection of OPs. Since organic solvents would destroy the biostructure of AChE and make it lose activity (remained enzyme activities are 11% and 5% after inhibition of biosensor-1 in pure ethanol and acetone for 5 min, respectively), both of the two biosensors were introduced for the detection of OPs in aqueous solution. Standard samples of OPs were prepared by diluting the stock solutions of OPs with doubly distilled water. Figure 2 shows the typical amperometric response of biosensor-1 to 0.2 mM acetylcholine before (curve a) and after inhibiting the biosensor in 10^{-5} g/L (curve b) and 10^{-9} g/L (curve c) parathion for 10 min.

Based on eqs 1 and 2, the inhibition rate and remaining enzyme activity could be calculated, where I_0 and I_1 represent the amperometric responses before and after the incubation procedure, respectively.

$$\text{Inhibition rate } \% = (I_0 - I_1)/I_0 \times 100\ \% \quad (1)$$

$$\text{Enzyme activity remaining } \% = I_1/I_0 \times 100\ \% \quad (2)$$

The inhibition and remaining AChE activity were calculated as 42.1% and 57.9% for 10^{-5} g/L parathion and 16.7% and 83.3% for 10^{-9} g/L parathion, respectively.

Two hypertoxic OPs, paraoxon and parathion, were detected with biosensor-1. Their moleculular structures are

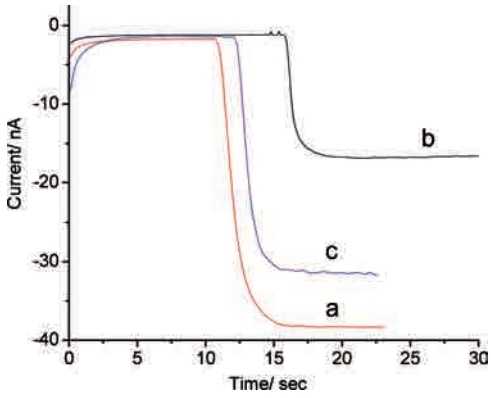

FIGURE 2. Amperometric responses of PDMS−PDDA/AuNPs/ChO/AChE modified electrode before (a) and after inhibition in 10^{-5} g/L (b) and 10^{-9} g/L (c) parathion for 10 min to 0.20 mM acetylcholine in a stirring 0.1 M pH 9.0 borate buffer under 0.7 V.

shown in Figure S3. Incubation time is another important factor for this system. For biosensor-1, the dependence of inhibition on incubation time with different concentrations (1×10^{-9}, 1×10^{-5}, 1×10^{-2} g/L) of paraoxon and parathion was examined at 25 °C and is shown in Figure S4. Ten min was chosen as optimal incubation time. For biosensor-2, the inhibition time was also chosen as 10 min. We also investigated the influence of temperature to the inhibition time. At 4 °C, the incubation time increased significantly and required almost 20 min to acheive a stable inhibition rate. Therefore, the incubation temperature was chosen as 25 °C.

Under the optimal conditions established in the above studies, calibration plots were generated for paraoxon and parathion (Figure 3A, curve a and b) based on biosensor-1. The relative inhibition of AChE activity is increasing with the concentration of paraoxon ranging from 10^{-10} to 10^{-2} g/L and is linearly with -log [paraoxon] at the concentration range of 10^{-9} to 10^{-2} g/L ($y = (106.2 \pm 1.8) - (9.7 \pm 0.3)x$, $r = 0.997$), with a detection limit down to 5×10^{-10} g/L (calculated for 15% inhibition rate). The linear range and detection limit for parathion are 10^{-9} to 10^{-2} g/L ($y = (107.7 \pm 2.4) - (10.6 \pm 0.4)x$, $r = 0.996$) and 10^{-9} g/L, respectively. As a sensitive amperometric biosensor, the detection limit for paraoxon and parathion are 3 orders lower than those from the fiber-optic AChE-inhibition biosensor (*13*). In addition, compared with the biosensor based on carbon nanotube modified thick film strip electrode for paraoxon detection, the detection limit of biosensor-1 is 400 times lower (*17*). Therefore, for the detection of hypertoxic OPs, biosensor-1 shows excellent sensitivity.

Further experiment showed that OPs with lower toxicity could hardly inhibit the activity of AChE. For example, methamidophos, with 5 times lower lethal dose than parathion, showed slight inhibition of AChE activity (Figure 3A, curve c). Other low toxic OPs such as dimethoate (Figure 3A, curve d), sumithion (Figure 3A, curve e), malathion, and trichlorfon (not shown) barely influenced the AChE activity.

There was no report that the neurotransmitter enzyme, AChE has any selectivity to special OPs. Therefore, we made biosensor-2 for comparison. Figure 3B, shows that the detection of paraoxon and parathion by biosensor-2 is as sensitive as that by biosensor-1. As shown in curves a and b for paraoxon, the linear range and detection limit are 10^{-9} to 10^{-3} g/L ($y = (112.6 \pm 3.7) - (10.7 \pm 0.6)x$, $r = 0.993$) and 4×10^{-10} g/L, respectively; for parathion, they are 10^{-9} to 10^{-3} g/L ($y = (110.1 \pm 2.7) - (10.7 \pm 0.4)x$, $r = 0.996$) and 4×10^{-10} g/L, respectively. However, biosensor-2 does not show any selectivity to OPs. The relative inhibition of AChE activity is increasing with the concentration of methamidophos ranging from 10^{-10} to 10^{-2} g/L and is linearly with -log [methamidophos] in the range from 10^{-8} to 10^{-5} g/L ($y = (152.0 \pm 11.3) - (16.8 \pm 1.7)x$, $r = 0.990$). The linear ranges for the detection of sumithion and dimethoate are 10^{-6} to 10^{-3} g/L ($y = (111.9 \pm 6.2) - (17.0 \pm 1.3)x$, $r = 0.994$) and $10^{-8} - 10^{-2}$ g/L ($y = (97.6 \pm 3.0) - (11.7 \pm 0.6)x$, $r = 0.994$).

Here we found the interesting phenomenon that biosensor-1 showed unique selectivity to hypertoxic OPs. This makes the biosensor perfect for monitoring banned OPs. As for biosensor-2, it could work as a common applicable AChE-inhibition biosensor for the detection of most OPs. We tried to figure out the reason of this performance in the following section.

Elaboration of the Structure of AChE Molecule-Oriented Immobilization. Figure 4A shows the space-filling stereo view of the AChE molecule. The active site is composed of two subsites: the esteratic subsite (red) which contains the catalytic triad, and the anionic subsite (cyan) (*31*). The active site is located in a cavity of AChE molecule and named as the "active site gorge" by Sussman and co-workers (*32*). Fourteen aromatic residues line a substantial portion of the surface of the gorge (green).

In 1970, Kabachnik et al. reported the localization of the hydrophobic areas on the active surface of AChE (*31*). They demonstrated the general idea of three hydrophobic areas near the catalytic center of AChE and investigated the peculiarities of these areas. Now, it is well-known that the high aromatic content of the active site gorge explains the hydrophobic binding sites around active site, and the hydrocarbon and aromatic side-chain amino acids construct all the hydrophobic areas of AChE (*31*). From the space-filling stereo view of the AChE molecule looking down upon the active site (Figure 4B), it can be seen that the hydrophobic areas (orange) are much denser around the active site gorge than at other places such as the inverse side (Figure 4C). Therefore, it is likely that AChE would adopt different orientations when immobilizing on hydrophobic or hydrophilic surfaces. On a hydrophobic surface, AChE should be primarily adsorbed via hydrophobic interaction, which results in the active site gorge facing down to the surface. This orientation may protect the enzyme activity better and increase the physical obstruction to OPs. Conversely, on the hydrophilic surface, the active site should mainly face upward due to the repulsion between the hydrophobic residues of enzyme (Figure 4D). Other driving forces such as electrostatic attraction and hydrogen bond could work for the adsorption.

OPs are electrophilic compounds that phosphorylate the serine hydroxyl group located in the active site of AChE. The phosphorylation yields a stable, inactive enzyme. The basic chemical structure of OPs is described by Schrader's formula (see Figure S3A). Substituents at R_1 and R_2 are alkyl, alkoxy, alkylthio, or amino groups, and the substituent at X is a labile acyl residue (halide, cyano, phenol, or thio group). The structural diversity of OPs is due to different substituents at the phosphorus atom. The reactivity of OPs varies upon the chemical structure. Electrophilicity of the phosphorus atom is crucial for the biological actions of OPs. High electrophilicity at the phosphorus atom corresponds to a high reactivity of OPs and a strong binding to the active site of AChE. Therefore, the AChE inhibition depends on two important factors: the reactivity of OPs and the steric hindrance for OPs to attack the active site of AChE. An allosteric structure or a special orientation of AChE on solid surface may increase the steric hindrance for the attraction from OPs. Based on the molecular structure of AChE and the surface properties of the PDMS−PDDA/AuNPs film, it is possible to assume that the enzyme would adopt different orientations when

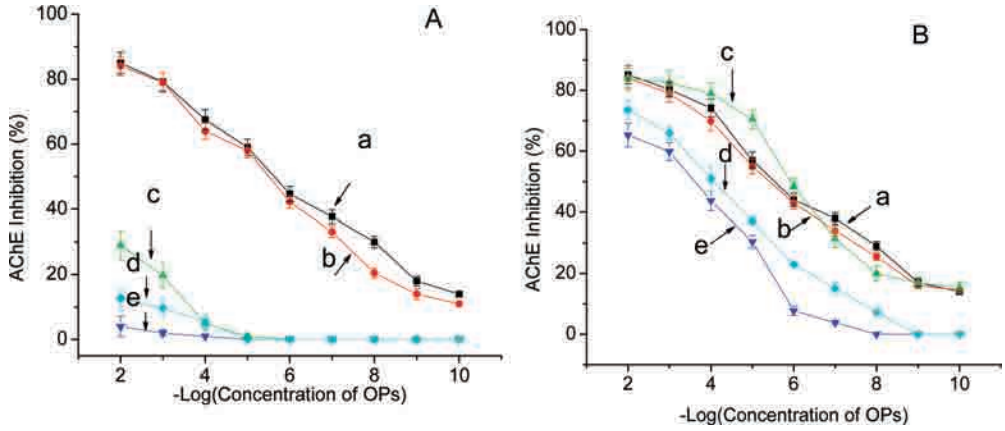

FIGURE 3. Inhibition curves of the biosensor-1 (A) and biosensor-2 (B) to different concentrations of paraoxon (a), parathion (b), methamidophos (c), dimethoate (d), and sumithion (e). Inhibition was performed in aqueous solution for 10 min with OPs.

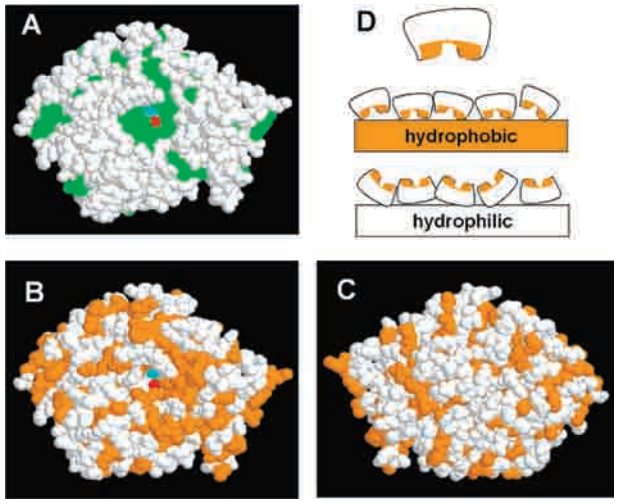

FIGURE 4. Space-filling stereo view of the AChE molecule looking down into the active site gorge. (A) Aromatic residues are green, and other residues are light gray. Ser^{200} (red) and Glu^{199} (cyan) are visible toward the bottom of the gorge; (B) hydrophobic residues are orange, the colors of other residues are the same as A; (C) the inverse side of B; (D) Schematic representations of the possible molecular orientations of AChE immobilized onto the hydrophobic and hydrophilic surfaces. The active site gorge is shown as an opening and hydrophobic areas close to the active site are indicated by orange.

immobilized on hydrophobic and hydrophilic surfaces, and the active site gorge of AChE would face upward or downward to the electrode. Consequently, the access to the active site of AChE for enzyme substrate and inhibitors should be different. In this case, it is assumed that for OPs with lower toxicity, the steric-hindrance effect is dominant. Therefore, they failed in the inhibition of AChE of biosensor-1. For hypertoxic OPs with high electrophilicity, their high reactivity is the dominance factor. Therefore, we get a selective detection of hypertoxic OPs with biosensor-1.

Real Sample Analysis: Detection of Omethoate Residue in Cottomrose Hibiscus Leaves. Dimethoate is one of the widely used pesticides for agricultural and household applications with moderate toxicity. It has solubility up to 39 g/L in water under room temperature. Dimethoate can be accumulated in leaves and is a main pollution source to Chinese tea (*33*). Studies show that the nutritive value of fishes exposed to dimethoate is significantly influenced. Therefore, importance should also be attached to controlling dimethoate pollution to aquatic plants and animals that play important roles in food chains (*34*). As an

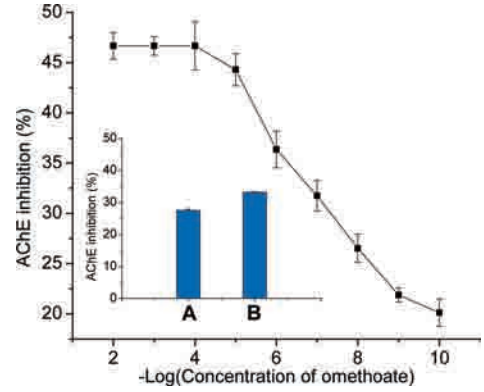

FIGURE 5. Inhibition curves of the biosensor-1 with different concentrations of omethoate. Inserts: A: Inhibition of biosensor-1 to omethoate in samples; B: inhibition of biosensor-1 to omethoate in samples with added 1.3 $\times$ 10^{-7} g/L omethoate standard solution.

insecticide and acaricide, dimethoate exhibits both contact and systemic activity. As one kind of organophosphorus pesticides, it also elicits toxicity by inhibiting the enzyme acetylcholinesterase. When applied to plants or adsorbed by animals, dimethoate could be easily oxidized into omethoate (see molecule structure of omethoate in Figure S3), which is a hypertoxic pesticide and would do harm to humans with a comparatively high concentration. Thus, it is important to monitor omethoate residues. Herein, the PDMS−PDDA/AuNPs/ChO/AChE based biosensor-1 was utilized to analyze omethoate residue on Cottomrose Hibiscus leaves. The calibration plot was generated for omethoate (Figure 5) based on biosensor-1 with fresh standard solutions of omethoate prepared in doubly distilled water immediately before use. The relative inhibition increased with the concentration ranging from 10^{-10} to 10^{-2} g/L and was linearly with -log [omethoate] at the concentration range of 10^{-9} to 10^{-4} g/L ($y = (68.3 \pm 1.9) - (5.2 \pm 0.3)x$, $r = 0.994$). The Cottomrose Hibiscus was sprayed with dimethoate in the morning (6 a.m.). The leaves were collected within 4 h (9−10 a.m.), and accurately weighed (14.6466 g) and extracted with 50 mL of pH 7.0 PBS. Biosensor-1 was incubated in the extracted solution for 10 min and then made quantitative detection and calculation. The concentration of dimethoate in the extracted solution was examined with HPLC, and the concentration was calculated as less than 2.3×10^{-5} g/L via external standard method. Dimethoate with concentration less than 10^{-4} g/L would barely introduce any inhibition to biosensor-1 (see Figure 3A, curve d). Therefore, the inhibition was from the omethoate. The omethoate

content in the extracted solution were calculated as 1.3×10^{-8} g/L with the RSD of 1.4% ($n = 3$), and the recoveries of omethoate added to the real samples were from 98.6% to 107.7%, indicating an acceptable accuracy.

Acknowledgments

This research was supported by the NSFC (grant 20890021), the NSFC for Creative Research Groups (grant 20821063), the 973 Program (2007CB936404) and the program for New Century Excellent Talents in University (NCET).

Supporting Information Available

Typical amperometric response of biosensor-1; effects of pH and temperature on the responses of the twin biosensors; Schrader's formula for organophosphorus compounds; structures of paraoxon, parathion, and omethoate; AChE activity in response to OPs at different exposure times. This material is available free of charge via the Internet at http://pubs.acs.org.

Literature Cited

(1) Rosenberry, T. L. *Advances in Enzymology and Related Areas of Molecular Biology*; John Wiley & Sons: New York, 1975.

(2) Fennouh, S.; Casimiri, V.; Burstein, C. Increased paraoxon detection with solvents using acetylcholinesterase inactivation measured with a choline oxidase biosensor. *Biosens. Bioelectron.* **1997**, *12*, 97–104.

(3) Guerrieri, A.; Monaci, L.; Quinto, M.; Palmisano, F. A disposable amperometric biosensor for rapid screening of anticholinesterase activity in soil extracts. *Analyst* **2002**, *127*, 5–7.

(4) Liu, G. D.; Lin, Y. H. Electrochemical sensor for organophosphate pesticides and nerve agents using zirconia nanoparticles as selective sorbents. *Anal. Chem.* **2005**, *77*, 5894–5901.

(5) UNEP/FAO/PIC/ICRC.4/10/Add.2 12. *Inclusion of chemicals in the interim prior informed consent procedure- Review of notifications of final regulatory actions to ban or severely restrict a chemical*; December 2002.

(6) UNEP/FAO/RC/CRC.1/19 10. *Inclusion of chemicals in Annex III of the Rotterdam Convention: review of notifications of final regulatory actions to ban or severely restrict a chemical: methyl parathion*; December 2004.

(7) Sherma, J. Pesticides. *Anal. Chem.* **1993**, *65*, 40R–54R.

(8) Pylypiw, H. M. Rapid gas chromatographic method for the multiresidue screening of fruits and vegetables for organochlorine and organophosphate pesticides. *J. AOAC Int.* **1993**, *76*, 1369–1377.

(9) Sadik, O.; Land, W.; Wang, J. Chemical and biological warfare agents at the molecular level. *Electroanalysis* **2003**, *15*, 1149–1159.

(10) Liu, G. D.; Lin, Y. H. Biosensor based on self-assembling acetylcholinesterase on carbon nanotubes for flow injection/amperometric detection of organophosphate pesticides and nerve agents. *Anal. Chem.* **2006**, *78*, 835–843.

(11) Du, D.; Huang, X.; Cai, J.; Zhang, A. D. Amperometric detection of triazophos pesticide using acetylcholinesterase biosensor based on multiwall carbon nanotube-chitosan matrix. *Sens. Actuators B: Chem.* **2007**, *127*, 531–535.

(12) Arduini, F.; Ricci, F.; Tuta, C. S.; Moscone, D.; Amine, A.; Palleschi, G. Detection of carbamic and organophosphorous pesticides in water samples using a cholinesterase biosensor based on Prussian Blue-modified screen-printed electrode. *Anal. Chim. Acta* **2006**, *580*, 155–162.

(13) Mulchandani, A.; Pan, S.; Chen, W. Fiber-optic biosensor for direct determination of organophosphate nerve agents. *Biotechnol. Prog.* **1999**, *15*, 130–134.

(14) Pardio, V. T.; Ibarra, N.; Rodriguez, M. A. Use of cholinesterase activity in monitoring organophosphate pesticide exposure of cattle produced in tropical areas. *J. Agric. Food Chem.* **2001**, *49*, 6057–6062.

(15) Sole, S.; Merkoci, A.; Alegret, S. Determination of toxic substances based on enzyme inhibition. Part I. Electrochemical biosensors for the determination of pesticides using batch procedures. *Crit. Rev. Anal. Chem.* **2003**, *33*, 89–96.

(16) Lin, Y.; Lu, F.; Wang, J. Disposable carbon nanotube modified screen-printed biosensor for amperometric detection of organophosphorus pesticides and nerve agents. *Electroanalysis* **2004**, *16*, 145–149.

(17) Joshi, K.; Tang, J.; Haddon, R.; Wang, J.; Chen, W.; Mulchandani, A. A disposable biosensor for organophosphorus nerve agents based on carbon nanotubes modified thick film strip electrode. *Electroanalysis* **2005**, *17*, 54–58.

(18) Sotiropoulou, S.; Chaniotakis, N. A. Lowering the detection limit of the acetylcholinesterase biosensor using a nanoporous carbon matrix. *Anal. Chim. Acta* **2005**, *530*, 199–204.

(19) Jeanty, G.; Ghommidh, Ch.; Marty, J. L. Automated detection of chlorpyrifos and its metabolites by a continuous flow system-based enzyme sensor. *Anal. Chim. Acta* **2001**, *436*, 119–128.

(20) Jeanty, G.; Marty, J. L. Detection of paraoxon by continuous flow system based enzyme sensor. *Biosens. Bioelectron.* **1998**, *13*, 213–218.

(21) Wang, X.; Zhou, D.; Sinniah, K.; Clarke, C.; Birch, L.; Li, H.; Rayment, T.; Abell, C. Electrostatic orientation of enzymes on surfaces for ligand screening probed by force spectroscopy. *Langmuir* **2006**, *22*, 887–892.

(22) Patrito, N.; McCague, C.; Norton, P. R.; Petersen, N. O. Spatially controlled cell adhesion via micropatterned surface modification of poly(dimethylsiloxane). *Langmuir* **2007**, *23*, 715–719.

(23) Lee, J. H.; Chung, S.; Kim, S. J.; Han, J. Poly(dimethylsiloxane)-based protein preconcentration using a nanogap generated by junction gap breakdown. *Anal. Chem.* **2007**, *79*, 6868–6873.

(24) Mata, A.; Fleischman, A. J.; Roy, S. Characterization of polydimethylsiloxane (PDMS) properties for biomedical micro/nanosystems. *Biomed. Microdevices* **2005**, *7*, 281–293.

(25) Zhao, W.; Sun, S. X.; Xu, J. J.; Chen, H. Y.; Cao, X. J.; Guan, X. H. Electrochemical identification of the property of peripheral nerve fiber based on a biocompatible polymer film via in situ incorporating gold nanoparticles. *Anal. Chem.* **2008**, *80*, 3769–3776.

(26) Zhang, Q.; Xu, J. J.; Liu, Y.; Chen, H. Y. In-situ synthesis of poly(dimethylsiloxane)/gold nanoparticles composite films and its application in microfluidic systems. *Lab Chip* **2008**, *2*, 352–357.

(27) Bourdillon, C.; Majda, M. Microporous aluminum oxide films at electrodes. 7. Mediation of the catalytic activity of glucose oxidase via lateral diffusion of a ferrocene amphiphile in a bilayer assembly. *J. Am. Chem. Soc.* **1990**, *112*, 1795–1799.

(28) Zhao, W.; Xu, J. J.; Shi, C. G.; Chen, H. Y. Multilayer membranes via layer-by-layer deposition of organic polymer protected prussian blue nanoparticles and glucose oxidase for glucose biosensing. *Langmuir* **2005**, *21*, 9630–9634.

(29) Cosnier, S.; Innocent, C. Detection of Galactose and Lactose by a Poly(Amphiphilic Pyrrole)-Galactose Oxidase Electrode. *Anal. Lett.* **1994**, *27*, 1429–1442.

(30) Morra, M.; Occhiello, E.; Marola, R.; Garbassi, F.; Humphrey, P.; Johnson, D. On the aging of oxygen plasma-treated polydimethylsiloxane surfaces. *J. Colloid Interface* **1990**, *137*, 11–24.

(31) Kabachnik, M. I.; Brestkin, A. P.; Godovikov, N. N.; Michelson, M. J.; Rozengart, E. V.; Rozengart, V. T. Hydrophobic areas on the active surface of cholinesterases. *Pharmacol. Rev.* **1970**, *22*, 355–388.

(32) Sussman, J. L.; Harel, M.; Frolow, F.; Oefner, C.; Goldman, A.; Toker, L.; Silman, I. Atomic structure of acetylcholinesterase from *Torpedo californica*: a prototypic acetylcholine-binding protein. *Science* **1991**, *253*, 872–879.

(33) Lv, Y. Q.; Lin, Z. X.; Feng, W.; Zhou, X.; Tan, T. W. Selective recognition and large enrichment of dimethoate from tea leaves by molecularly imprinted polymers. *Biochem. Eng. J.* **2007**, *36*, 221–229.

(34) Begum, G.; Vijayaraghavan, S. Alterations in the protein metabolism of muscle tissue in fish, *Clarias batrachus* (Linn.) by commercial grade dimethoate. *Bull. Environ. Contam. Toxicol.* **1996**, *57*, 223–228.

ES900841N